# Mechanical Characterization and Shape Optimization of Fascicle-Like 3D Skeletal Muscle Tissues Contracted with Electrical and Optical Stimuli

By Devin Neal, Mahmut Selman Sakar, Rashid Bashir, Vincent Chan and H. Harry Asada*

[*]Dr. Devin Neal, Dr. Vincent Chan, Prof. H. Harry Asada
Department of Mechanical Engineering
Massachusetts Institute of Technology
77 Massachusetts Avenue, Room 1-007, MA 02139 (USA)
E-mail: asada@mit.edu

Prof. Rashid Bashir
Electrical and Computer Engineering
University of Illinois at Urbana-Champaign
1270 Digital Computer Lab MC 278
1304 W. Springfield
Urbana Illinois 61801

Dr. Mahmut Selman Sakar
Institute of Robotics and Intelligent Systems
ETH Zurich
Zurich, CH 8092 (Switzerland)

## *Abstract*

Here we present a quantitative approach to constructing effective 3D muscle tissues through shape optimization and load impedance matching with electrical and optical stimulation. We have constructed long, thin, fascicle-like skeletal muscle tissue and optimized their form factor through mechanical characterization. A new apparatus was designed and built which allowed us to measure force-displacement characteristics with diverse load stiffnesses. We have found that a) there is an optimal form factor that maximizes the muscle stress, b) the energy transmitted to the load can be maximized with matched load stiffness, and c) optical stimulation using channelrhodopsin2 in the muscle tissue can generate twitch force as large as its electrical counterpart for well developed muscle tissue. Using our tissue construct method we found an optimal initial diameter of 500 microns outperformed tissues using 250 microns by more than 60% and tissues using 760 microns by 105%. Using an optimal load stiffness, our tissues have generated 12 pJ of energy per twitch at a peak generated stress of 1.28 kPa. Additionally, the difference in optically stimulated twitch performance vs. electrically stimulated is a function of how well the overall tissue performs, with average or better performing strips having less than 10% difference. The unique mechanical characterization method used is generalizable to diverse load conditions and will be used to match load impedance to muscle tissue impedance for a wide variety of applications.

## *Introduction*

Formation of an engineered skeletal muscle tissue in-vitro can have a range of engineering and medical applications. Successful construction of such a muscle tissue can not

only shed light on the muscle formation process [Rhim et al., 2007], but can also open the door to creating organ mimics for drug screening and drug development replacing expensive animal models, especially if the essential mechanics and biology can be recapitulated in the in-vitro system. Similarly, developing in-vitro methodologies for muscle formation will allow engineers to build medical implants using biological materials [VanDusen et al., 2014], realize novel soft-robotics and biological machines, and interface these synthetic components with other naturally occurring systems.

To accomplish these goals, muscle constructs must act on a load, producing mechanical work and transmitting it to the load. Understanding of basic force-displacement characteristics and output power transmission is a pre-requisite for designing and building those machines and implants. Yet, quantitative and detailed mechanical work performance of in-vitro skeletal muscles has been reported only in a few articles but with a limited scope. This is primarily because of the complexity of muscle mechanics. The force generated by a muscle construct varies significantly depending on numerous conditions, including displacement, pre-stress, velocity, and load impedance as well as fatigue, creep and stress relaxation [Wang et al., 1993, Brooks et al., 1991, Gordon et al., 1996]. In the past, rather simple methods have been used for evaluating mechanical performance.

A common practice to characterize the muscle tissue is to measure the isometric tension generated. This is the measurement of the force generated while the tissue maintains a constant length by holding the two ends of the tissue at a constant position relative to each other throughout the measurement. The length may be maintained either by coupling it to rigid supports or by applying feedback position control of the ends. Feedback position control has been used as far back as 1965 when muscle from a live frog was tested to determine the relationship between sarcomere length and isometric tension generation [Gordon et al., 1966]. In vitro grown 3D muscle tissue constructs have been tested using stiff couplings [Dennis and Kosnik, 2000].

Isometric force measurements cannot provide information on the energy that can be imparted on a load for a single muscle twitch. Isometric force measurements are useful in finding peak forces achievable by muscle tissue, and in comparing muscle tissue formed under various conditions, such as testing effects of various influences like alignment, drugs, or damage. However, isometric force measurements cannot provide information on all time and displacement dependent parameters describing the muscle contraction such as power, or twitch energy. Twitch energy transmissibility is critically important for cardiac tissue, as well as for any engineered mechanical system powered by muscle tissue (biobots) [Chan et al., 2014].

With the addition of velocity control, a typical isometric muscle testing apparatus may be used to measure power output directly by testing isovelocity shortening [Brooks and Faulkner, 1991]. However, this power measured is dependent on the magnitude of the velocity, and a constant velocity is not necessarily the conditions in which the muscle will be functioning.

An alternative method of characterizing skeletal muscle tissue performance is to have the muscle tissue work against a load such as a known linear stiffness. With this aim, muscle tissue structures have been grown such that it's two terminal ends are supported by the ends of two compliant posts [Vandenburgh et al., 2008, Sakar et al., 2012, Boudou et al., 2012]. This method allows for the direct measurement of muscle tissue output energy transmitted to a load. However, the performance of any given tissue can only be assessed for driving a single load, i.e. the stiffness of the cantilevered posts. Fully characterizing the tissues against various loads is not possible with this method. Thus, the performance of the tissue under loads it may face in

physiological or engineered settings cannot be assessed directly from these prior reported structures. Additionally, it is impossible to remove the muscle tissue from the posts devices without damaging or altering its performance in the process. One final concern with using polymer posts is that their stiffness is influenced by many factors. The Young's Modulus of PDMS can change by roughly a factor of 2 simply by changing curing temperature [Johnston et al., 2007], and other factors such as temperature and deformation rate also change its compliance [Lotters et al., 1997]. Polymers are viscoelastic, therefor the resting stiffness must be measured separately from the short term, activation stiffness of polymer posts.

Here we present a systematic method and apparatus for evaluating the mechanical performance of in-vitro grown muscle constructs without using isometric contractions nor a single linear elastic load. The presented method allows for the testing of tissue performance against any load, and a single tissue sample may be tested against any number of loads. This method allows us to a) measure force-displacement characteristics, b) tune the pre-strain applied to the muscle construct, c) vary the stiffness of load impedance, and d) quantify the work produced by the muscle construct. Using this quantitative mechanical performance evaluation method, we address how 3D skeletal muscle constructs can be optimized with respect to a) form factor and morphology, and b) matching with the load stiffness. The primary objective of morphology evaluation here is to determine the optimal diameter at which to grow 3D, aligned muscle tissue having a high density of contractile proteins. We find that an optimal load impedance exists for a particular muscle construct to transmit the mechanical work. Specifically, performance is assessed in terms of maximum work transmitted to a load due to a single stimulated twitch cycle. Force and/or displacement may also be used in twitch performance comparison because these two values are monotonically coupled to the work performed.

The method of inducing contractions of muscle cells is another important factor when characterizing tissue. Three methods of stimulation have been used for engineered tissue characterization: chemical [Vandenburgh et al., 1991], electrical [Nagamine et al., 2011], and optical [Sakar et al., 2012]. Chemical and electrical stimulation involve potentially invasive changes to the cellular environment, and don't offer the same potential for tight spatial and temporal resolution as optical stimulation. Optical stimulation is a newer technique in which cells are transfected with DNA encoding the optogenetic protein channelrhodopsin2 (ChR2). Characterization of optical stimulation with comparison to an alternative form of stimulation has not been reported. The benefits of high spatial and temporal control of optogenetics over other forms of stimulation have already been used for high throughput testing *in vitro* [Sakar et al., 2012], and will eventually provide utility in clinical applications when combined with developing optical technologies [Kim et al., 2013].

The method presented here facilitates both electrical and optical stimulation for coherent comparison. It also facilitates the quantification of mechanical performance by elongating the tissue via lateral displacement. Lateral displacement entails displacing a tissue construct at a point between its two anchored ends in a direction perpendicular to the primary axis of the tissue. Lateral displacement for mechanical characterization has been used for neurite characterization [Dennerll et al., 1988] as well as for very simple skeletal muscle characterization [Vandenburgh et al., 1991]. Muscle tissue made via the sacrificial outer mold method described previously [Neal et al., 2014] facilitates this mechanical characterization method in two ways. First, the tissue is anchored between the stiff well walls of the culture device, ensuring no serial compliance at the anchor points that would affect measurements. This is in contrast to tissue developed on compliant posts. Second, the tissue can be tested without transferring the tissue to

another substrate or measurement device. This is in contrast to the methods of producing muscle constructs, which require at least one anchor to be decoupled from the culture dish on which the tissue is grown [Dennis and Kosnik, 2000]. Multiple cantilever probes of different stiffness may be used on a single tissue. This allows for the testing of tissue against different mechanical loads. Isometric and post based methods alone are incapable of testing a single tissue against differing loads. By changing the load, it is possible to determine the load impedance that matches the specific tissue to maximize the output work of the tissue. However, this method has never been used to characterize muscle tissue grown under varying conditions, nor with different cantilever probe stiffnesses and displacements.

## *Materials and methods*

### Muscle Strip Tissue Constructs

Fascicle-like muscle tissue constructs were produced as described previously [Neal et al. 2014]. For the experiments presented here, the sacrificial mold material consisted of 5% w/v porcine gelatin (Sigma-Aldrich), 10 U/ml thrombin (Sigma-Aldrich), and 1% 0.5 N NaCl in PBS (Lonza), and the cell solution consisted of 5 mg/ml fibrinogen (Sigma-Aldrich), $10^7$ cells/ml, and 0.5 mg/ml aminocaproic acid (Sigma-Aldrich). The cells used were C2C12 cells (ATCC) transfected with channel rhodopsin 2 (ChR2) as described previously [Sakar et al., 2012]. Growth media consists of 10% fetal bovine serum (Sigma-Aldrich) in DMEM (ATCC) and 0.5 mg/ml aminocaproic acid. Differentiation media contains 10% horse serum (Sigma-Aldrich), DMEM (ATCC) and 0.5 mg/ml aminocaproic acid.

Briefly, sacrificial mold material was injected at 37℃ into 5 mm diameter PDMS (Dow Corning) wells containing a steel pin (McMaster Carr) spanning the well. The mold material was then cooled to room temperature to solidify. Removal of the pins leaves a 5 mm long cylindrical cavity in the gelatin in the 5 mm diameter well.

This cavity is then filled with a cell/hydrogel solution. The device is then immediately placed in a 37℃ incubator where the gelatin mold melts releasing thrombin, and where the hydrogel solution solidifies. The sacrificial mold solution is then gradually diluted with daily media changing. Growth media is used for the first 2 days. Differentiation media is used after the first 2 days. Fascicle-like muscle constructs produced using this method are shown in Fig. 1a.

For the experiments in which pin diameter was the independent variable, two separate experiments were run. The first consisted of 3 devices with 2 strips in each device using each of the following nominal pin diameters: 0.010" (254 μm), 0.012" (305 μm), 0.014" (356 μm) and 0.020" (508 μm). The second consisted of 3 devices using each of the following nominal pin diameters: 0.014" (356 μm) and 0.020" (508 μm), 0.030" (762 μm), and 0.040" (1016 μm).

For the optical vs. electrical stimulation experiment, and the variable probe stiffness experiments 3 devices of 2 strips each were used, and nominal pin diameters used were 0.020" (508 μm).

For all experiments, stimulated contraction testing was performed 14 days after cell seeding.

### Force and Displacement Measurement Using a Lateral Cantilever Probe

The basic concept of the force probe is to laterally displace the tissue strip at its center using the end of a cantilever probe of known stiffness. As diagramed in Figs. 1b and 1c, the center of the tissue displaces in the direction orthogonal to the un-displaced tissue axis. As the

tip of the cantilever displaces the center of the strip, the length of the strip elongates, and the cantilever bends. Measuring the position of the cantilever base and tip, and knowing the stiffness of the cantilever, we can find the force of the probe, $F_{probe}$, exerted on the tissue:

$$F_{probe} = k_{probe}\left(x_{base} - x_{tip}\right) \quad (0)$$

where $x_{tip}$ is the lateral displacement of the cantilever tip, $x_{base}$ is the lateral displacement of the cantilever base, and $k_{probe}$ is the stiffness of the cantilever probe as shown in Fig. 1.

The geometric relationships relevant to displacement via a cantilever probes are shown in Supplementary Fig. S1. Combining geometric relations, force balance, and Hooke's law, we derive expressions for the axial force along the tissue, $F_{axial}$, and the displaced length of half the tissue, $L'$. From the diagram:

$$\frac{F_{axial,x}}{F_{axial}} = \frac{x_{tip}}{L'} \quad (0)$$

$$x_{tip} = \sqrt{L'^2 - L^2} \quad (0)$$

where $F_{axial,x}$ is the lateral component of the axial force held by the tissue, and $L$ and $L'$ are the unforced and forced half-lengths of the tissue, respectively.

A simple force balance along the direction of displacement is:

$$F_{probe} = 2F_{axial,x} \quad (0)$$

Combining these equations yields an expression for the elongated length, $L'$, and axial force, $F_{axial}$, of the tissue:

$$L' = \sqrt{{x_{tip}}^2 + L^2} \quad (0)$$

$$F_{axial} = \left(x_{base} - x_{tip}\right)\frac{k_{probe}}{2x_{tip}}\sqrt{{x_{tip}}^2 + L^2} \quad (0)$$

From these equations, we can determine both axial force of the tissue, and tissue elongation.

## Characterization System

For this concept to work, 1) we must be able to finely adjust the position of the base of the cantilever, $x_{base}$, 2) the positions of the cantilever base, $x_{base}$, and tip, $x_{tip}$, must be measured simultaneously, and 3) the muscle tissue must be excitable. A new custom built system that achieves these requirements is presented in Fig. 2. The base of the cantilever is positioned with a 3-axis stage assembly, coupled to the cantilever probe via a stiff custom machined aluminum beam. For the 3-axis stage assembly, x position (probe displacement direction) is controlled using both a manual stage (Thorlabs MT1/M) and a motorized stage (Thorlabs MT1/M-Z8), and y and z positions are controlled with a 2-axis manual stage (Thorlabs DT12XZ/M). The 3-axis stage assembly is rigidly mounted to the microscope stage. The probe cantilevers and electrodes are super glued to easily interchangeable 3D printed couplings that easily snap onto the end of the aluminum beam in a repeatable manner. This quick snap method allows for numerous cantilever probes of any desired stiffness to be quickly interchanged while collecting data. The position of the base of the cantilever is measured with a laser micrometer (Micro-Epsilon optoNCDT 1401), which measures the position of a 3D printed laser micrometer flag attached to the aluminum beam that extends away from the sample. The position of the tip is measured via

images from a microscope. Video recorded on the microscope computer coupled with the time history data from the laser micrometer are combined to give time dependent data. In order to excite the muscle tissue electrically, electrodes that are attached to the cantilever base extend into the sample well and terminate with ends that are parallel to the strip.

Cantilever stiffnesses were evaluated before and after testing to ensure the stiffnesses were consistent and that they were not plastically deformed during testing. The stiffnesses were evaluated by hanging known weights from the tip against gravity.

For all experiments, multiple twitches were generated via stimulation at the same pre-strain conditions. In this system, pre-strain was created by laterally displacing the cantilever probe to the point where approximately 2% strain was generated along the direction of the tissue strip. The base of the probe is fixed, and then contraction stimuli are applied.

This system is a general force transducer and may be adapted to other applications demanding measurements of small forces and small displacements, such as characterization of microposts [Sakar et al., 2012], or other biological materials. The only adaptation necessary for these and other applications would be to produce 3D printed couplings with probes specific to the application.

In order to provide electrical stimulation to the muscle strips, electrodes were built into the system that would be capable of providing an electric field across the strip. Platinum electrodes are parallel to the strip to generate a uniform field across its length. The electrodes are at the precise depth of the tissue and independent of the displacement of the tissue as shown in Fig. S4a. The depths of the electrodes and probe tip are mechanically coupled to ensure the depths of the electrodes and the probe tip are the same. To allow the probe tip and tissue to move independently of the electrodes upon displacement, compliant cantilevered electrodes rigidly coupled to the base of the cantilever tip were used. The electrodes are platinum wires coupled closely to the cantilever tip, and that splay out away from the cantilever probe as they extend down. When unforced, the two electrodes are separated by approximately 3 times the width of the sample well at their ends (Fig. S4b). When inserted into the sample well, the electrodes must first be brought together with tweezers (Fig. S4c). The elastic energy stored in the compliant electrodes keeps them pinned to the walls of the sample well even as the system translates the cantilever probe (Fig. S5).

For electrical stimulation, an electric field of 30 V/cm was used with bipolar pulses of 1 ms each, at a frequency of 1 Hz. The electric signal was controlled by an Arduino Uno microcontroller with custom scripts. For optical stimulation, a 300-W mercury lamp coupled with a GFP (473 nm wavelength) was used to generate 30 ms pulses at 1 Hz using custom scripts written into the microscope controlling software (Metamorph).

The magnitude of the stimulation, both optical and electrical was selected to be high enough such that a 25% reduction in stimulation strength had no measurable change in stimulation caused response. To address the concern of tissue penetration of the light stimulus, we made sure that the entire depth of tissue could be imaged using the stimulation strength of the light source. It is confirmed that because the tissue can be well imaged, stimulating light can penetrate the tissue.

## Optical vs. Electrical Stimulation Response Characterization

A single cantilever and pair of electrodes were used in the optical vs. electrical stimulation experiments. The optical vs. electrical stimulation protocol was designed to account for the effects of muscle fatigue. If we simply stimulated one way and then the other, muscle

fatigue would make the second stimulation method appear worse due to fatigue of the strip. 6 stimulation cycles were performed for each strip with 60 seconds of rest between each. Each stimulation cycle consisted of two sub cycles with 60 seconds of rest between each. Each sub-cycle consisted of pre-straining the tissue, stimulating the tissue 5 times with one form of stimuli (electric or optical) followed immediately by stimulating the tissue 5 times with the other form of stimuli (optical or electric), then relaxing the tissue. Using this protocol, muscle fatigue is factored out through averaging over all cycles. This protocol is shown in Supplementary Fig. S2. The stiffness of the cantilever used was 0.0278 N/m.

## Tissue Response vs. Varying Loads Characterization

4 different cantilevers with different stiffnesses were used in the variable stiffness experiment. Each strip was tested with each cantilever twice using the following protocol: the strip was displaced by the cantilever tip to a pre-strained value of 2% strain and stimulated 5 times optically, then relaxed. For the diameter variation experiments, the protocol was the same as the variable stiffness experiment protocol, except only 1 cantilever probe was used. The stiffnesses used in the variable stiffness experiment were the following: 0.0038 N/m, 0.023 N/m, 0.11 N/m, and 0.65 N/m.

## Tissue Response as a Function of Diameter Characterization

A single cantilever and pair of electrodes were used in the diameter variation experiments. Each strip was used to generate 5 twitches. The stiffness of the cantilever used was 0.0278 N/m.

## Image and Video Analysis

Data from the laser micrometer (measuring cantilever probe base position) and the microscope camera video (measuring cantilever tip position) was processed to generate axial tissue force and displacement. The video data provides probe tip data with the use of open source software called Tracker. Tracking the cantilever tip is robust and reliable giving sub-pixel resolution. Each individual twitch was analyzed independently. This process is shown in Supplementary Fig. S3. The tip and base data are synchronized based on a step-like input to the base position. Each twitch is segmented and combined with probe base data to determine axial strip displacement and force. Finally, each twitch is creep corrected assuming linear creep with a slope equal to the post twitch position minus the pre-twitch initial tip position divided by the twitch time. This creep correction is used to ensure that the data presented represent the force and displacements generated only by the contraction of the muscle.

## Statistical Analysis

In determining statistically significant differences, the means are compared using 2 sampled t-tests.

## *Results*

### Optical vs. Electrical Stimulation

Electric stimulation performance was slightly superior to optical stimulation performance overall. Fig. 3 shows the wave forms and peak values of twitch forces induced by both optical and electrical stimuli. The peak force values of 5 twitches were evaluated for optical and electrical stimuli, and for each of 6 muscle strips having diverse levels of performance. The difference in the mean peak twitch force was less than 10% for stronger muscle strips. However, for poor performing strips, optical stimulation resulted in almost 40% worse mean twitch amplitude than electrical stimulation. Twitch data for the best performing strip, strip A (Fig. 3a) and the worst performing strip, strip C (Fig. 3b) exemplify this. The optically stimulated twitches nearly follow the electrically generated twitches for the high performing strip, strip A, while the optically generated twitches are generally much lower in force than the optically generated twitches for the poor performing strip, strip C. Aggregate data of the maximum twitch force generated for multiple strips with various overall performance (Fig. 3c) show that electric stimulation is mildly superior to optical stimulation. A trend can clearly be seen when the aggregate of the ratio of optical to electrical stimulation performance for each strip is plotted against mean maximum twitch force of the electrically stimulated twitches for each strip (Fig. 3d). This clearly demonstrates that, as the overall performance of the strip increases, the relative performance of optically generated twitches approaches the performance of electrically generated twitches.

These results show that muscle constructs developed to a certain level may be stimulated optically and electrically with similar resulting contractions. This means that optical control of muscle tissue may be used for stimulation purposes in situations where electrodes are too intrusive or otherwise disadvantageous.

### Maximum Stress and Optimal Diameter

In Fig.4 multiple strips with diverse diameters are compared with respect to peak twitch force and stress. The largest twitch force was generated by the strip whose nominal pin diameter was 762 μm rather than 1016 μm (Fig. 4b). In terms of maximum peak stress, i.e. peak force divided by the cross-sectional area, the 508 μm nominal diameter pin produced the maximum stress (Fig. 4a). The stress performance quickly drops off after this as the diameter increases. These results show that an optimal diameter exists for generating maximum stress. For the constructs formed using the smaller diameters (254, 305, and 356 microns), the mean stress generated is approximately the same and is independent of initial diameter.

Note that the standard deviation in peak twitch stress is much greater for the smallest diameter pins used (Fig. 4a). There exists a greater degree of non-uniformity for the smaller diameter strips, as described previously [Neal et al., 2014]. Fig. 5 shows the confocal images of the strips and their cross-sections. The diameter of the strip varies along the longitudinal direction. The cross-section at the end of the small diameter strip (Fig. 5a) contains only one myotube (shown as a colored circle), while the center cross-section has at least 3 myotubes. The local stiffness of the narrow region tends to be lower than that of thicker regions. Narrower regions of the construct act as compliant elements connected in series with the rest of the construct. These compliant "weak links" absorb displacement with the elastic tissue, decreasing the resulting output force (Fig. 4b). The larger diameter strips have more uniform cross-sections throughout the strip, leading to the larger force generation (Fig. 5b).

## Generated Energy and Load Matching

The twitches of a single muscle construct working against multiple cantilever probes of diverse stiffnesses are shown in Fig. 6. Each data point represents the combination of peak twitch displacement and force measured with a single probe. The stiffer the cantilever, the larger the peak twitch force and lower the peak twitch displacement (Fig. 6a). A linear fit matches the force-displacement curve with an $r^2$ value of 0.955. This shows that the higher the impedance of a load, the higher the maximum force of the tissue, but the lower the displacement. The peak energy stored in the cantilever probe resulting from a twitch is equal to half of the product of the peak twitch force and peak twitch displacement. For a linear relationship between force and displacement, the energy output as a function of displacement is a parabola with a global maximum in the middle (Fig. 6b). This energy maximum represents the maximum energy that a single twitch can transmit to a linear elastic load, such as the cantilever probe.

The performance of an engineered muscle construct and the impedance of the load it will drive should match in order for the muscle to transmit the most energy per contraction cycle to the load. This is clearly shown in Fig. 6b. There is a maximum energy transmission when the cantilever with an intermediate stiffness of 0.023 N/m is used. Notice that the energy transmitted to the stiffest cantilever results in the highest force, but not the highest energy transmission of the four probes used. Thus, the system presented here has been used to find an impedance that maximized the output energy and that it is not equal to the impedance that produces the maximum output force.

## *Discussion*

Using the mechanical characterization system described here, three key observations about engineered muscle constructs have been made. First, optical stimulation of myotubes formed from cells transfected with ChR2 encoding DNA is potentially as powerful as electrical stimulation if the muscle constructs are developed sufficiently. Second, there exists an optimal form factor at which to grow muscle tissue constructs seeded in a 3D scaffold where the performance metric is contraction performance per unit volume. Third, there exists an optimal load impedance to drive with an individual muscle construct where the performance metric is energy transmission to a load.

The key observation about optical stimulation broadens the potential use of optically stimulated muscle tissue. Muscle tissue that can be optically stimulated has been presented, but has not yet been methodically compared to electrical stimulation [Sakar et al., 2012]. The proposed benefits of optical stimulation over electrical stimulation include having no need to use potentially invasive electrodes, and the high spatial-temporal accuracy in stimulating specific muscle cells that may exist near other muscle cells. However, a significant question existed about the performance of optical stimulation. We show here that, if the performance of the muscle tissue is average or above, optical and electrical stimulus produce similar twitches. This is likely due to superior strips having more highly developed contractile myotubes. This results in a greater proportion of functional myotubes that are not optically excitable. Another possibility that has not been shown explicitly is that immature/poor performing myotubes may need a greater level of stimulation than optical stimulation can provide. Further exploring this phenomenon may provide valuable insights on how myotubes develop. With the results presented here, knowing that optical stimulation can produce similar results to electrical stimulation, future research may be conducted with optogenetic muscle tissue without the potential concern for vastly inferior performance.

The next key observation is about optimal form factor. There is an optimal strip diameter that produces the maximum twitch stress due to two conflicting requirements for the strip diameter. One is that the contractile cell density decreases as diameter increases, and the other is that the uniformity of strip cross-section decreases as the diameter decreases. These two phenomena can be put together in the simple linear component model shown in Fig. 5 to predict the results in Fig.4.

Considering the first phenomenon, for larger diameter strips, diffusion limiting processes discourage myotube formation within the central region of the construct yielding fewer myotubes per cross sectional area. This has been shown previously [Neal et al. 2014] where the volume of α-actinin is used as a surrogate of myotube volume. Additionally, if there are fewer cells near the central region to degrade the scaffold, then more scaffold will exist in the central region, resulting in increased passive scaffold the tissue must work against, as diagramed in Fig. 5c. A simple model of this first phenomenon assumes the cross section of the tissue has two regions, 1) an outer annulus of contractile tissue, and 2) an inner disk of non-contractile scaffold. In the model, the thickness of the contractile ring/annulus is assumed to be ~100 μm. When the thickness of the construct is this value or lower, all of the tissue is modeled as contractile. As the thickness of the construct becomes larger, a non-contractile region in the center begins to grow. Reported values of fibrin stiffness (~1 kPa) were used to model this inactive region [Duong et al., 2009]. The contractile region is modeled as producing ~1 kPa of peak stress based on observation and previous research [Dennis et al., 2000], and the stiffness of the cantilever load that the tissue is working against is modeled as ~0.01 N/m, which is similar to the stiffness used to gather the data. This model of the effects of cell density results in the descending regions of the full model plotted in Figs. 4c and 4d, where final tissue diameter > 150 μm.

The other phenomenon modeled is the greater degree of non-uniformity for smaller diameter constructs. This is modeled as compliant elements in series as shown in Figure 5 where exemplary strips are shown. Significant nonuniformities exist for smaller diameter strips because forces generated by individual myotube formation and development generates significant stress that causes necking of the hydrogel material lacking in differentiated myotubes. This does not happen in thicker constructs because the larger cross sectional area of hydrogel is able to resist necking as individual myotubes mature over time. The overall stiffness is dominated by the most compliant elements. It has previously been reported that variation of the smallest strips (250 micron initial diameter) vary in diameter by 25% [Neal et al., 2014]. The effect of diameter non-uniformity on stiffness can be modeled as two springs in series having different stiffnesses. If the strip is simply modeled as 2 halves with one having 75% of the mean diameter, and the other having 125% of the mean diameter, then the effective stiffness of this structure is ~65% of a uniform structure having a constant diameter, under the assumption that stiffness is proportional to the diameter squared. This disparity decreases to zero as the initial pin diameter increases. This model of non-uniformity results in the decreasing performance as tissue diameter decreases. See the curves in Figs. 4c and 4d where final tissue diameter < 120 μm. While more detailed models are possible, this was the simplest model based on the physics of the system that captures the general trend observed in the twitch data. This same model fits well with both the stress and forces generated by the tissues.

Concerning the variation in twitch force between individual strips, there is greater variability in smaller construct twitch performance due in large part to the greater dependence on individual myotubes. Individual myotube performance varies from one cell to the next. The performance of the smaller diameter constructs varies more significantly than the larger

constructs which have a greater number of myotubes to average performance over as can be seen in Figs. 5a and 5b.

The best performing strip diameter was 500 microns and generated an average twitch stress of 1.28 kPa. This is in line with high performance muscle constructs reported in the literature [Huang et al. 2005, Lam et al. 2009, Hinds et al. 2011]. Using an optimal initial diameter of 500 microns, tissues outperformed tissues using 250 microns by more than 60% and tissues using 760 microns by 105%. It is important to note that some papers report maximum twitch stress generation using a modified area in their calculation. Hinds et al report a specific twitch force (stress generation) after they "normalize by the average cross-sectional area of the active muscle layer". Lam et al. report their specific twitch force using an "effective" diameter that is "the diameter of the constructs minus the area of the gel". The fact that research groups subtract the inactive central region of the tissue is in line with our findings of performance drop for larger diameter strips. It is important to also bear in mind that isometric force measurements which are those typically reported, will be larger than forces measured against a compliant load.

The existence of an optimal form factor implies that a full size skeletal muscle should be constructed as a bundle of the fascicle-like strips, each having the optimal diameter, rather than one monolithic bulk. As in-vivo muscles have a hierarchical structure, in-vitro grown skeletal muscles, too, should be constructed as a collection of optimal fascicle-like strips. When comparing twitch performance to other constructs made from bulk hydrogels, the directly measured generated stress is roughly twice as much. This is even more impressive given that the maximum stress measured in the system is not with isometric contractions, but with contractions against a compliant load, and that an immortalized cell line is used here rather than primary derived myocytes typically used in bulk hydrogel constructs which tend to have superior contraction performance to cell lines.

The final key observation is about characterizing a tissue to find an optimal impedance for energy transmission. By using the optimally stiff cantilever, 12 pJ of energy per twitch were transferred to the load. This demonstrates the utility of this unique tissue characterization platform. Further, more complex characterization of muscle tissue performance using this system is possible. This system may be used to characterize muscle tissue working against a wide variety of impedance loads from linear stiffness (as presented here) to non-linear, time-dependent loads relevant to tissue engineering. In its current state, the system cannot measure initial tension nor isometric tension because a measurable displacement is required to make a measurable force measurement, however, further advancements to the system to make these measurement and others is the subject of future work.

The cantilever probe loads presented are all simply linear elastic impedances, but don't need to be. Loads with dynamic impedance such as inertia and damping may also be implemented. Loads may include hydrodynamic conditions and/or highly nonlinear materials. The probe loading conditions may be made to match the loading conditions the tissue will be under when eventually put into use. Additionally, thanks to the similar performance to electrical stimulation, optical stimulation may be used to quickly and easily test any individual tissue under these arbitrary loading conditions. A valuable potential use will be testing constructs using cardiomyocytes instead of skeletal muscle cells. Cardiac muscle operates exclusively in a twitch-like manner and drives a hydrodynamic load as it pumps. Using this system, heart muscle tissue may be more fully characterized than isometric characterization can do alone.

The key findings of engineered muscle tissue as well as the characterization system presented here will be used to advance the field of muscle tissue research, muscle related drug

testing, and scaling engineered muscle constructs to produce muscle tissue systems of much larger size.

## *Acknowledgements*

This material is based on work supported in part by the National Science Foundation, under Grant No. CBET-0939511, the Science and Technology Center for Emergent Behaviors of Integrated Cellular Systems (EBICS), and in part by the Singapore-MIT Alliance of Research and Technology, BioSyM IRG.

## *References*

Boudou T, Legant WR, Mu A, Borochin MA, Thavandiran N, Radisic M, et al., "A microfabricated platform to measure and manipulate the mechanics of engineered cardiac microtissues," *Tissue Engineering Part A*, vol. 18, pp. 910-919, 2012.

Brooks SV, JA Faulkner, "Forces and Powers of Slow and Fast Skeletal Muscles in Mice During Repeated Contractions," Journal of Physiology, vol. 436, pp. 701-710, 1991.

Chan V, Jeong JH, Bajaj P, Collens M, Saif T, Kong H, et al., "Multi-material bio-fabrication of hydrogel cantilevers and actuators with stereolithography," *Lab Chip*, vol. 12, pp. 88-98, 2012.

Chan V, Asasda HH, Bashir R, "Utilization and control of bioactuators across multiple length scales," *Lab on a Chip*, vol. 14, pp. 653-670, 2014.

Dennis RG, and PE Kosnik, "Excitability and Isometric Contractile Properties of Mammalian Skeletal Muscle Constructs Engineered In Vitro," In Vitro Cellular & Developmental Biology, vol. 36, pp 327-335, 2000.

Dennerll TJ, HC Joshi, VL Steel, RE Buxbaum, and SR Heidemann, "Tension and Compression in the Cytoskeleton of PC-12 Neurites II: Quantitative Measurements," *Journal of Cell Biology*, vol. 107, pp. 665-74, 1988.

Gordon AM, AF Huxley, and FJ Julian, "The Variation in Isometric Tension With Sarcomere Length in Vertebrate Muscle Fibres," The Journal of Physiology, vol. 184, pp. 170-192, 1966.

Huang YC, RG Dennis, L Larkin, and K Baar, "Rapid formation of functional muscle in vitro using fibrin gels," *Journal of Applied Physiology,* vol. 98, pp. 706-713, 2005.

Johnston I, D McCluskey, C Tan, and M Tracey, "Mechanical characterization of bulk Sylgard 184 for microfluidics and microengineering," *J. Micromech. Microeng.*, vol. 24, p. 035017, 2014.

Kim T, JG McCall, YH Jung, X Huang, ER Siuda, et al., "Injectable, cellular-scale optoelectronics with applications for wireless optogenetics," *Science*, vol. 340, pp. 211-216, 2013.

Lam MT, Sim S, Zhu X, Takayama S, "The effects of continuous wavy micropatterns on silicone substrates on the alignment of skeletal muscle myoblasts and myotubes," *Biomaterials*, vol. 27, pp. 4340-4347, 2006.

Lam MT, Huang YC, Birla RK, Takayama S, "Microfeature guided skeletal muscle tissue engineering for highly organized 3-dimensional free-standing constructs," *Biomaterials*, vol. 30, pp. 1150-1155, 2009

Nagamine K, Kawashima T, Sekine S, Ido Y, Kanzaki M, Nishizawa M, "Spatiotemporally controlled contraction of micropatterned skeletal muscle cells on a hydrogel sheet," *Lab Chip*, vol. 11, pp. 513-517, 2011.

Neal D, Sakar MS, Ong LLS, Asada HH, "Formation of elongated fascicle-inspired 3D tissues consisting of high-density, aligned cells using sacrificial outer molding," *Lab on a Chip*, vol. 14, pp. 1907-1916, 2014.

Sakar MS, D Neal, T Boudou, MA Borochin, Y Li, R Weiss, RD Kamm, CS Chen and HH Asada, "Formation and optogenetic control of engineered 3D skeletal muscle bioactuators," *Lab on a Chip*, vol. 12, no. 23, pp. 4976-4985, 2012.

Rhim C, D Lowell, M Reedy, D Slentz, S Zhang, and W Kraus , et al., "Morphology and ultrastructure of differentiating three-dimensional mammalian skeletal muscle in a collagen gel," *Muscle Nerve*, vol. 36, pp. 71-80, 2007.

Vandenburgh HH, Swasdison S, Karlisch P, "Coputer-aided mechanogenesis of skeletal muscle organs from single cells in vitro," *FASEB J.*, vol. 13, pp. 2860-2867, 1991.

Vandenburgh H, J. Shansky, F Benesch-Lee, V Barbata, J Reid, and L Thorrez, et al., "Drug-screening platform based on the contractility of tissue-engineered muscle," *Muscle Nerve*, vol. 37, pp. 438-447, 2008.

Vandenburgh H, "High-content drug screening with engineered musculoskeletal tissues," *Tissue Eng: Part B*, vol. 16, pp. 55-64, 2010.

VanDusen KW, B. Syverud, M Williams, J Lee, and L Larkin, "Engineered Skeletal Muscle Units for Repair of Volumetric Muscle Loss in the Tibialis Anterior Muscle of a Rat," *Tissue Eng: Part A*, doi:10.1089/ten.TEA.2014.0060, 2014.

Wang K, McCarter R, Wright J, Beverly J, Ramirez-Mitchell R, "Viscoelasticity of the sarcomere matrix of skeletal muscles. The titin-myosin composite filament is a dual-stage molecular spring." *Biophys J.*, vol. 64, pp. 1161-1177, 1993.

Figure Captions

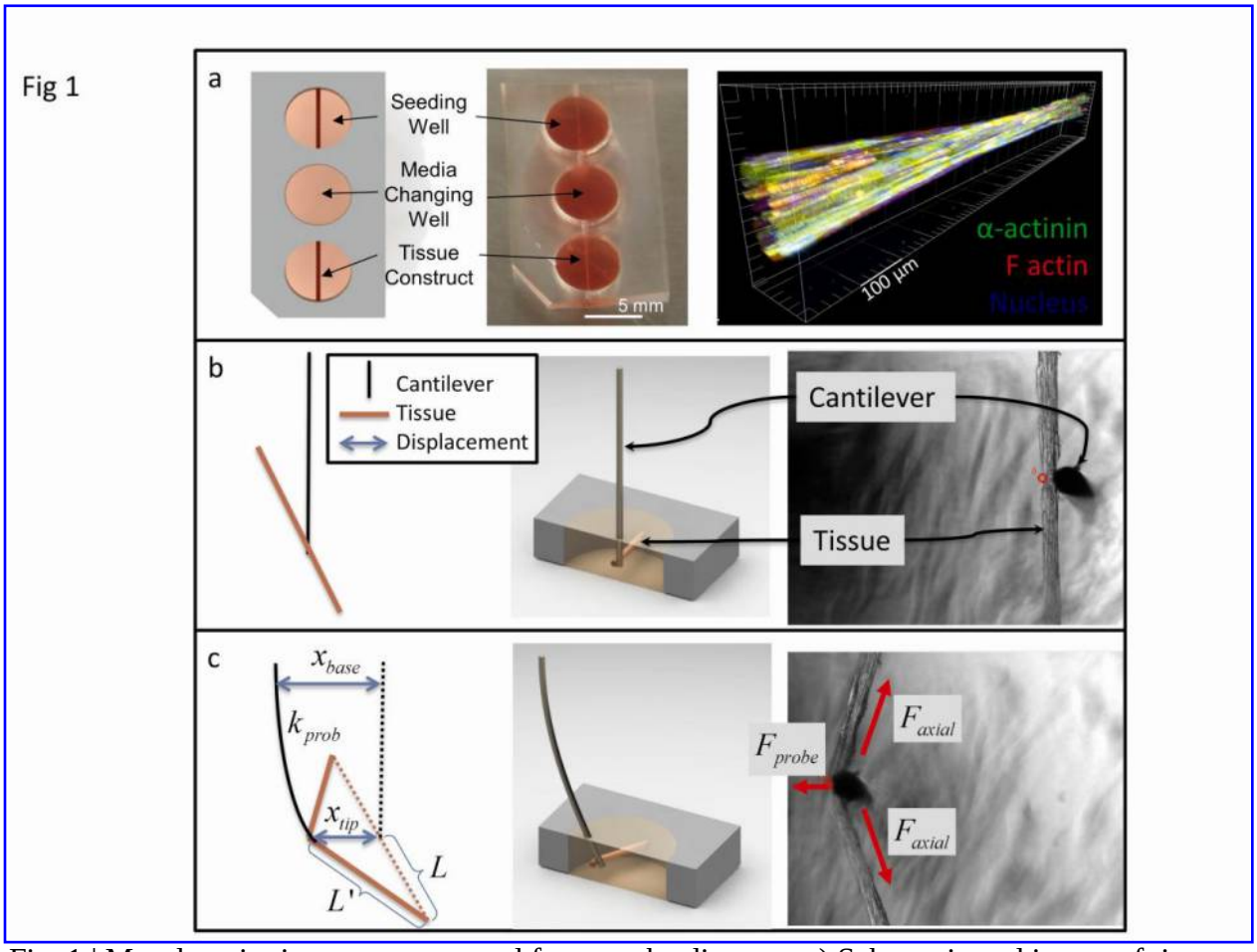


Fig. 1 | Muscle strip tissue construct and force probe diagram. a) Schematic and image of tissue culture device, along with confocal image of muscle strip consisting of numerous muscle cells in a device. b) Diagram, solid model, and image of cantilever in contact with tissue with no displacement. c) Diagram, solid model, and image of cantilever tip displacing tissue due to displacement of cantilever base. $x_{tip}$ is the lateral displacement of the cantilever tip, $x_{base}$ is the lateral displacement of the cantilever base, and $k_{probe}$ is the cantilever stiffness. $L$ and $L'$ are the unforced and forced half-lengths of the tissue, respectively. $F_{probe}$ is the force on the probe tip, and $F_{axial}$ is the force along the axis of the tissue.

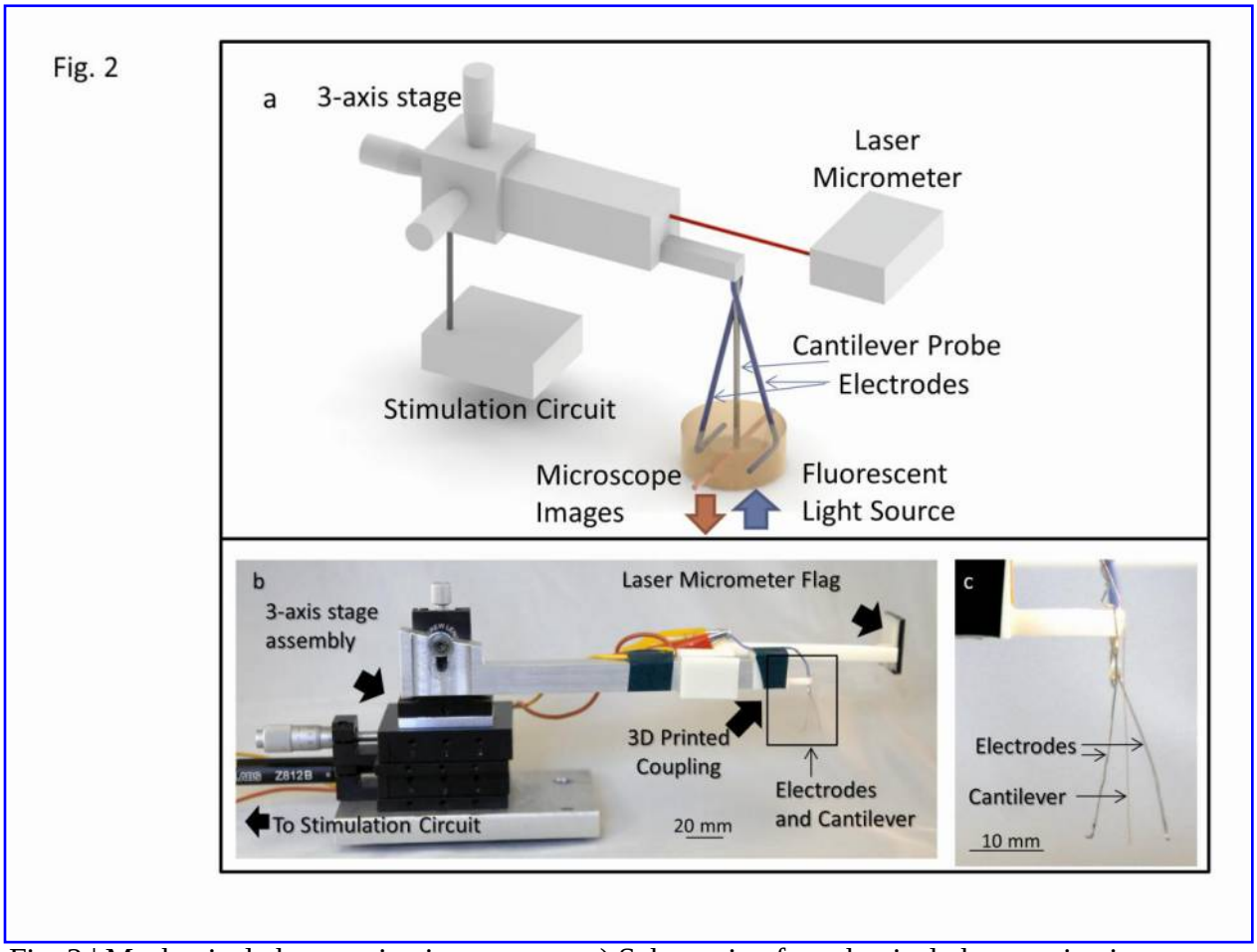


Fig. 2 | Mechanical characterization system. a) Schematic of mechanical characterization system. b) Key components of mechanical characterization system. c) A 3D printed tip with a cantilever probe and electrodes.

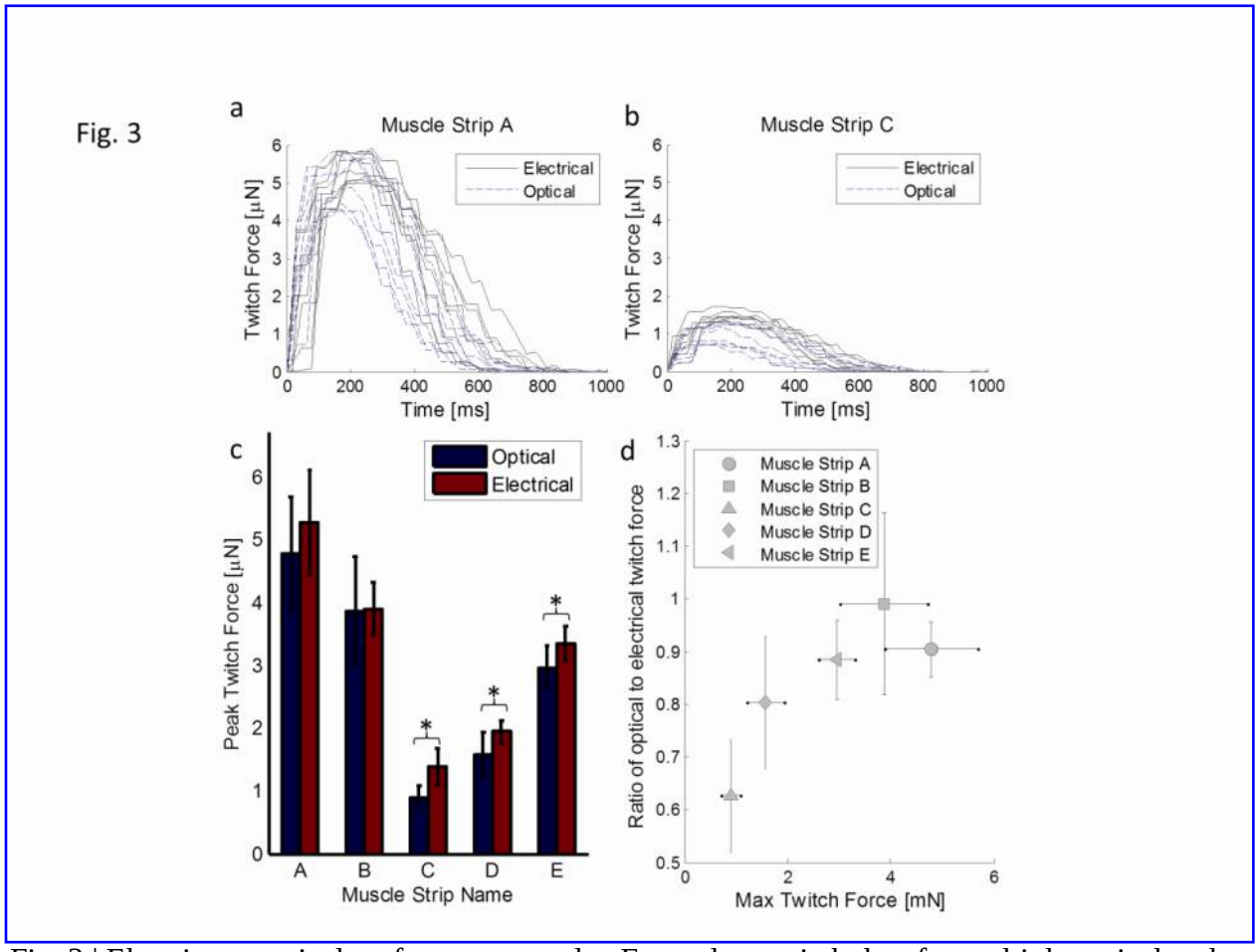


Fig. 3 | Electric vs. optical performance results. Exemplary twitch data for multiple optical and electrically stimulated twitches for a better than average performing strip (a) and less than average performing strip (b). c) Aggregate data of maximum twitch force achieved for numerous twitches stimulated via electrical and optical signals. d) The ratio of optically to electrically stimulated maximum twitch force plotted against mean maximum twitch force generated electrically. Asterisks represent statistical differences with $p < 0.05$. Error bars are standard deviation values and n is 30 for each sample set.

Fig. 4

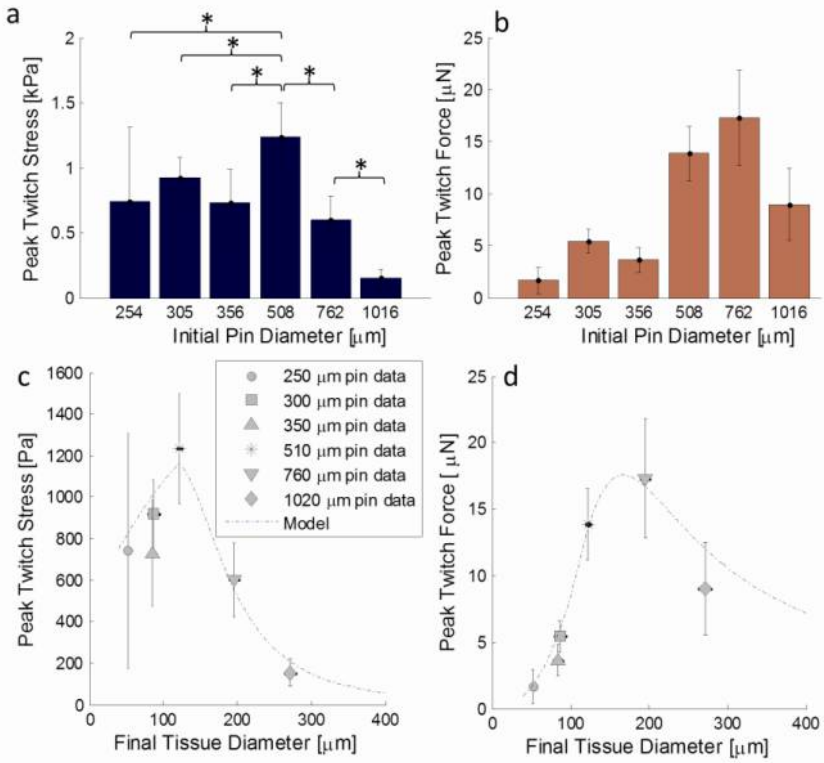


Fig. 4 | Peak twitch stress and force over various initial pin diameters. Peak stress (a) and force (b) from twitches generated by constructs made using various initial nominal diameter pins. Initial pin diameter is a key controlled variable in maximizing final tissue stress output and is shown in (a) and (b) to emphasize the statistical significance of the peak stress magnitude achieved when using a pin diameter of 508 microns. Asterisks represent statistically significant differences with $p<0.05$. Peak twitch stress (c) and force (d) plotted against final construct diameter from constructs of differing initial pin diameter and a simple model that assumes 1) greater variability in tissue diameter along length for smaller diameter tissues, and 2) only the outer ~50 microns of construct produce significant contractile stress due to diffusion limited processes during development. Compaction of the tissue from initial pin diameter to final tissue diameter is more dramatic for smaller diameter molds. All error bars are standard deviations and n is 30 for each sample set.

Fig. 5

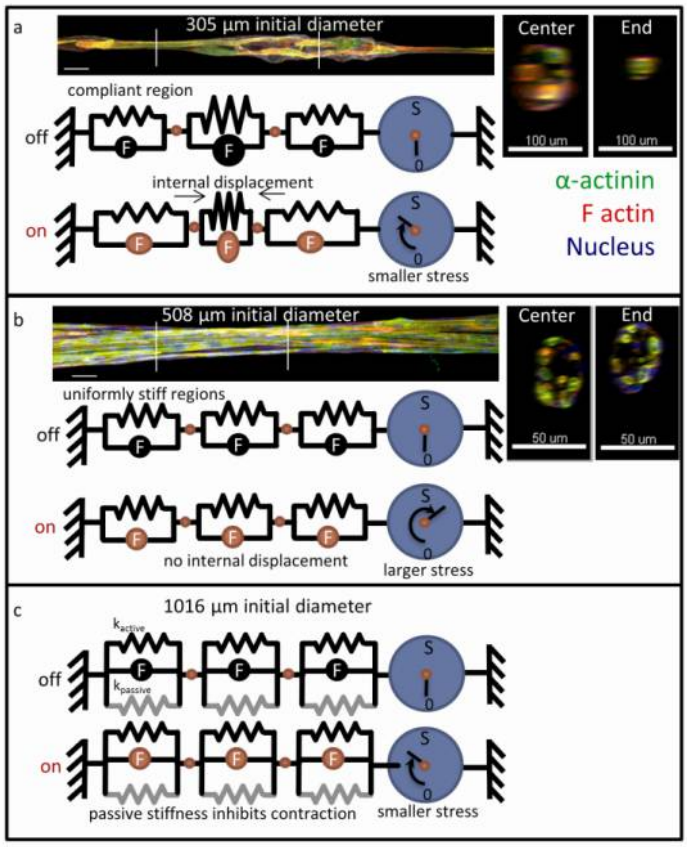


Fig. 5 | Compliance model. Diagram of consequences of nonuniform strip development (a) vs. uniform strip development (b) showing that compliant regions in tissue result in internal displacements of the tissue that decrease the muscle's transmission of mechanical energy to an external load. (c) As the diameter increases, there is a greater volume of passive material that acts as a stiffness to decrease contraction stress generation. Unspecified scale bars are 50 µm.

Fig. 6

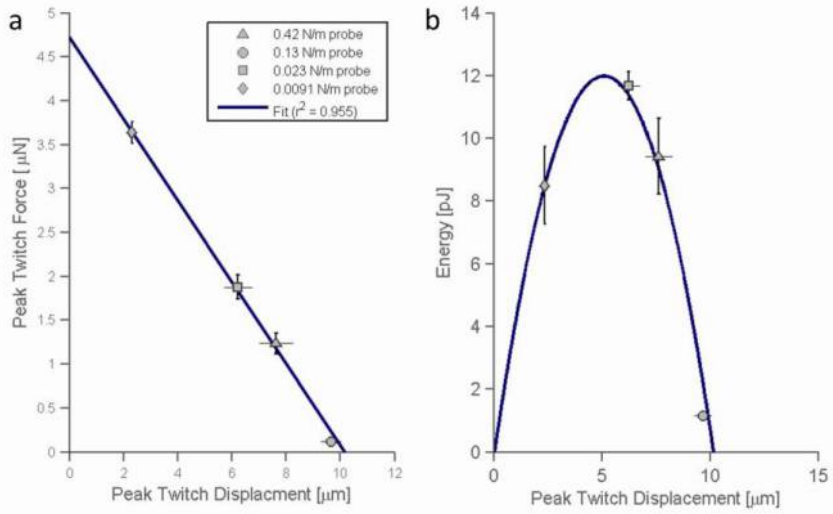


Fig. 6 | Tissue performance under varying load conditions of a typical well performing construct. a) Peak twitch force and peak twitch displacement for a single tissue stimulated while laterally pulling the tissue with 4 different cantilevers of different stiffness. b) Peak energy stored in the probe cantilever as a function of tissue displacement under 4 different cantilever loads. The straight line in a) is a linear regression fit to the force-displacement data, while the parabola in b) is the fit derived from the linear regression found in A). The max. energy is produced in the middle of the force-displacement characteristics. Note: probe stiffness values are not equal to the geometry corrected effective stiffness seen by the tissue. Error bars represent standard deviation. Error bars are smaller than symbol where not shown.

Fig. S1

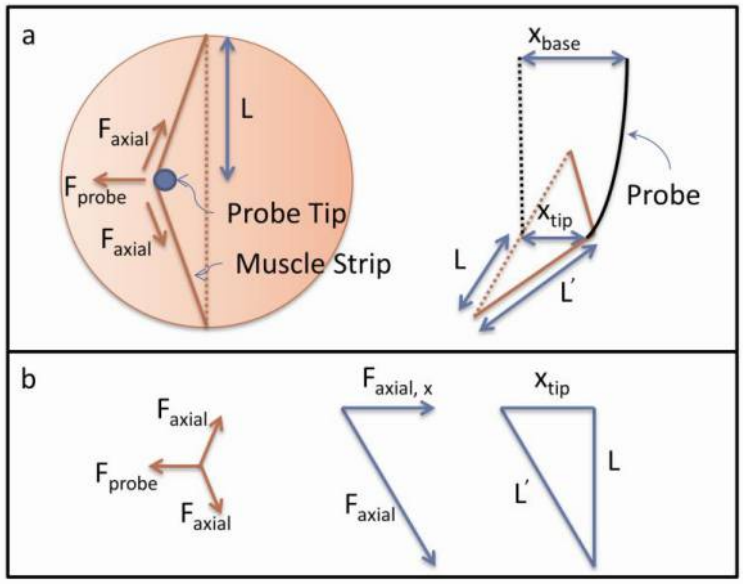


Fig. S1 | Force probe diagram. a) Free body diagram of cantilever tip when a tissue is displaced and a diagram with labeled lengths of the cantilever and tissue. b) Simplified free body diagram and length relationships. $F_{probe}$ is the force on the probe tip, and $F_{axial}$ is the force along the axis of the tissue. $x_{tip}$ is the lateral displacement of the cantilever tip, $x_{base}$ is the lateral displacement of the cantilever base. $L$ and $L'$ are the unforced and forced half-lengths of the tissue, respectively.

Fig. S2

# Stimulation protocol

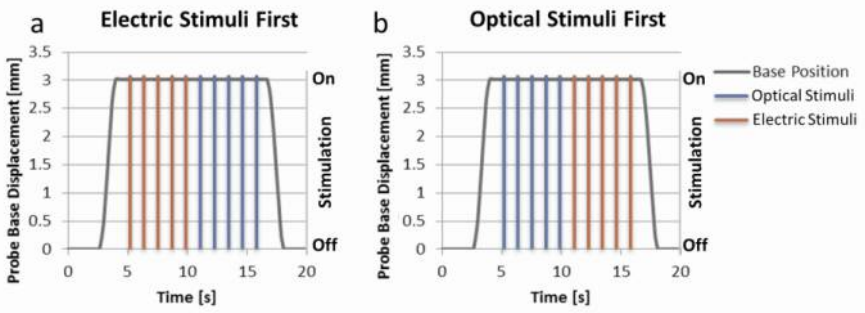


c

| Stimulation Cycle | First Sub Cycle | Second Sub Cycle |
|---|---|---|
| First | Electric Stimuli First | Optical Stimuli First |
| Second | Optical Stimuli First | Electric Stimuli First |
| Third | Electric Stimuli First | Optical Stimuli First |
| Fourth | Optical Stimuli First | Electric Stimuli First |
| Fifth | Electric Stimuli First | Optical Stimuli First |
| Sixth | Optical Stimuli First | Electric Stimuli First |

Fig. S2 | Stimulation protocol. For the electric vs. optical stimulation experiment, stimulation sub-cycles consisted of either electric stimuli first (a) or optical stimulation first (b). These cycles were repeated alternatively in six full stimulation cycles (c) with 60 s of rest between each sub-cycle.

Fig. S3

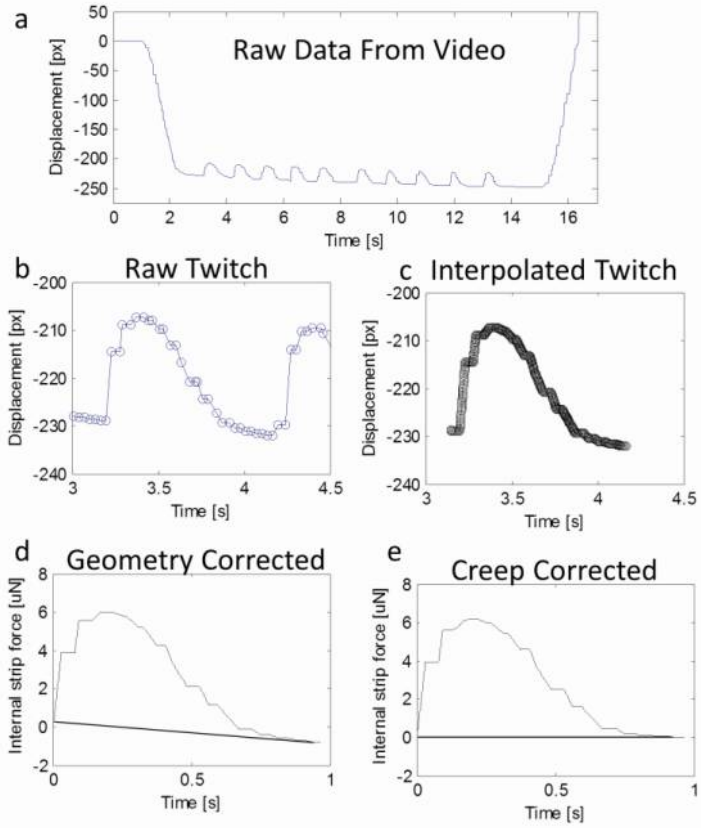


Fig. S3 | Twitch data analysis. a) Raw probe tip data is generated from video processing software. b) Individual twitch data. c) Raw data is interpolated for point-to-point matching with probe base data recorded with a laser micrometer. d) Interpolated twitch data from base and tip data sets are geometrically combined to generate data for the axial force of the tissue. e) Twitch data is adjusted for the slight creep occurring during the twitch assuming a constant creep rate.

Fig. S4

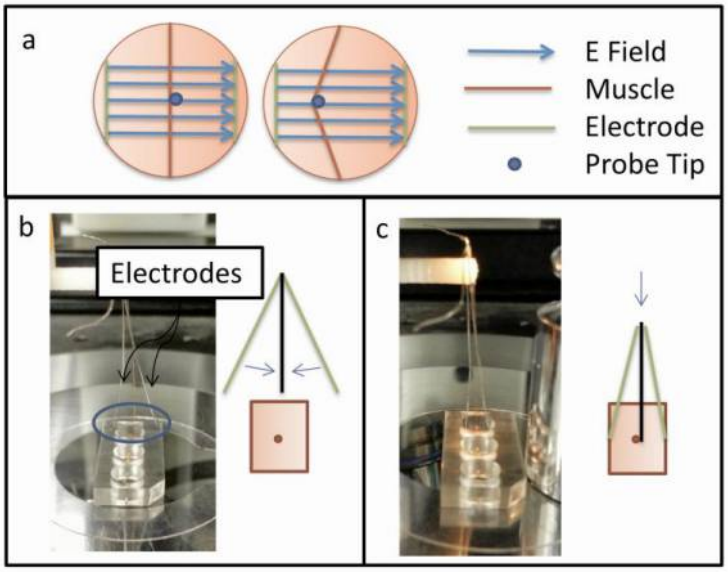


Fig. S4 | Electrode design. a) Top view of tissue well showing electric field lines independent of probe tip displacement in which electrodes do not move as probe tip displaces tissue. b) Image and side view diagram of compliant electrodes above tissue well. c) Image and sideview diagram of compliant electrodes inserted into tissue well. Well diameters are 5 mm.

Fig. S5

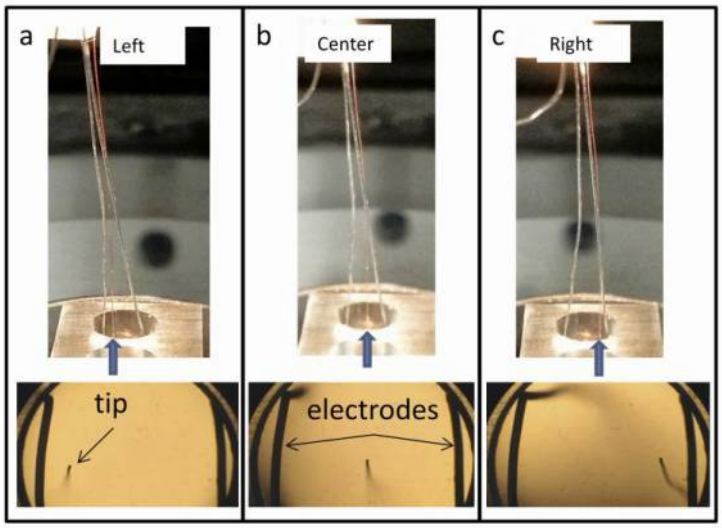


Fig. S5 | Compliant electrodes functioning. As the cantilever tip is displaced to the left (a), center (b), and right (c) of a well, the compliant electrodes do not lose contact with the well walls.